Effect of Sr doping on the magnetocapacitive effect in $Bi_{0.6}Sr_{0.4}FeO_{3-\delta}$ polycrystalline ceramics

R. Rajesh, S. John Ethilton, K. Ramachandran, K. Ramesh Kumar, Samba Siva Vadla & I. B. Shameem Banu

Applied Physics A
Materials Science & Processing

ISSN 0947-8396
Volume 124
Number 8

Appl. Phys. A (2018) 124:1-9
DOI 10.1007/s00339-018-1941-6

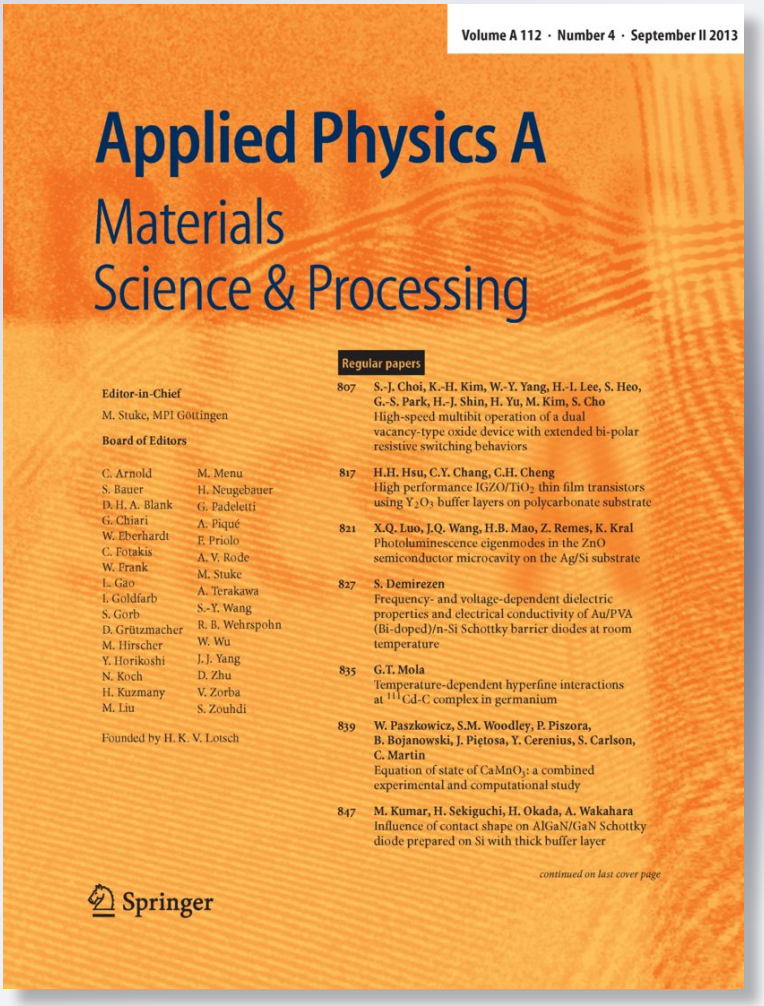

Springer

Your article is protected by copyright and all rights are held exclusively by Springer-Verlag GmbH Germany, part of Springer Nature. This e-offprint is for personal use only and shall not be self-archived in electronic repositories. If you wish to self-archive your article, please use the accepted manuscript version for posting on your own website. You may further deposit the accepted manuscript version in any repository, provided it is only made publicly available 12 months after official publication or later and provided acknowledgement is given to the original source of publication and a link is inserted to the published article on Springer's website. The link must be accompanied by the following text: "The final publication is available at link.springer.com”.

Author's personal copy

Applied Physics A (2018) 124:532
https://doi.org/10.1007/s00339-018-1941-6

Applied Physics A
Materials Science & Processing

Effect of Sr doping on the magnetocapacitive effect in $Bi_{0.6}Sr_{0.4}FeO_{3-\delta}$ polycrystalline ceramics

R. Rajesh[1] · S. John Ethilton[1] · K. Ramachandran[2] · K. Ramesh Kumar[3] · Samba Siva Vadla[4] · I. B. Shameem Banu[5]

Received: 16 March 2018 / Accepted: 29 June 2018
© Springer-Verlag GmbH Germany, part of Springer Nature 2018

Abstract
Single-phase polycrystalline $BiFeO_3$ and $Bi_{0.6}Sr_{0.4}FeO_{3-\delta}$ are prepared by conventional solid-state route. The host $BiFeO_3$ shows rhombohedral phase (*R3c*) and $Bi_{0.6}Sr_{0.4}FeO_{3-\delta}$, cubic phase (*Pm3m*). The *M–H* loop of $Bi_{0.6}Sr_{0.4}FeO_{3-\delta}$ exhibits weak magnetization at ambient temperature with saturation magnetization of 5.097 emu/g which is almost two orders larger in magnitude than in $BiFeO_3$ (0.088 emu/g). The temperature-dependent dielectric permittivity of $Bi_{0.6}Sr_{0.4}FeO_{3-\delta}$ shows a strong anomaly at 321 °C, a signature of magnetoelectric coupling present in this material and the magnetocapacitance effect is found to be 5.3% at a field of 4 kOe.

1 Introduction

Multiferroic materials are the special class of materials exhibiting two or more ferroic ordering such as ferroelectric, ferromagnetic, ferroelastic and ferrotoroidic in the same phase [1]. The linear coupling between magnetic and electric polarizations in multiferroics can produce a number of additional functionalities, such as magnetocapacitive effect and/or magnetoelectric effect in which the magnetization can be induced by the applied electric fields and vice versa [2]. It is known that all the multiferroic materials are not magnetoelectric and vice versa, but $BiFeO_3$ is one such material with multiferroic as well as magnetoelectric properties having a distorted ABO_3-type perovskite structure. It possesses antiferromagnetic ordering below 370 °C and ferroelectric below 830 °C [3]. $BiFeO_3$ has only limited industrial applications due to the formation of secondary phases during synthesis and producing an inhomogeneous spin structure leading to high leakage current and weak magnetization [4]. To reduce the leakage current and for using in variety of applications, researchers have attempted doping in *A* (viz. Bi) and/or *B* (viz. Fe)—sites by leaching, sintering, etc., in $BiFeO_3$ [5–7]. Partial substitution of trivalent metal ions on *A*-site will help to increase the electric and magnetic behaviour [5, 8], whereas partial substitution of divalent metal ions such as Sr^{2+}, Pb^{2+}, Ba^{2+}, Ca^{2+} and Co^{2+} in the *A*-site of $BiFeO_3$ might stabilize the system in cubic or tetragonal perovskite structure with considerable reduction in the secondary phases [9, 10]. Similarly, avoiding secondary phases substitution of alkaline metal ion like Sr^{2+} on $BiFeO_3$ is also recommended by researchers because this can produce high magnetic field-induced electric polarization. For example, Singh et al. [11] reported improved ferroelectric polarization of $2P_r = 86.13$ μC/cm^2 in Sr-doped $BiFeO_3$ thin films. Mandal et al. [12] reported nanostructured multiferroic $Bi_{1-x}Sr_xFeO_3$ ($0 \le x \le 0.5$) through gel-combustion via magnetic field-induced dielectric permittivity. Varshney et al. [13] reported polycrystalline $Bi_{1-x}Sr_xFeO_3$ ($0 \le x \le 0.25$) with magnetoelectric coupling. Kundys et al. [14] reported a maximum polarization of $P_r = 96$ μC/cm^2 at a field of 10 T when $Bi_{0.75}Sr_{0.25}FeO_{3-\delta}$ is in *pm-3m* cubic phase. Thakur et al. [15] claimed that polycrystalline $Bi_{1-x}Sr_xFeO_3$ ($0 \le x \le 0.3$) creates Fe^{4+} valence ions to maintain the charge neutrality and creates defects and/or oxygen vacancies in the system. But when the concentration of Sr starts increasing from 40%, the system crystallizes into *p4mm* phase and shows more oxygen vacancies with higher conductivity

✉ R. Rajesh
rr@vcet.ac.in

1 Department of Physics, Velammal College of Engineering and Technology, Madurai 625009, India

2 Department of Physics, Gandhigram Rural Institute Deemed University, Gandhigram, Dindigul 624 302, India

3 Department of Physics, University of Johannesburg, PO Box 524, Auckland Park 2006, South Africa

4 Department of Physics, Indian Institute of Technology Madras, Chennai 600 036, India

5 Department of Physics, B.S. Abdur Rahman University, Chennai 600 048, India

Published online: 10 July 2018

Author's personal copy

and thermal stability. Balamurugan et al. [16] claimed that $Bi_{0.5}Sr_{0.5}FeO_3$ remains in the *R3c* phase with coexistence of ferromagnetism and ferroelectricity at ambient temperature. Hussain et al. [17] observed a dielectric anomaly in the *pm3m* cubic phase of $Bi_{1-x}Sr_xFeO_3$ ($0 \le x \le 0.45$) when the concentration of Sr is 35 and 45% in $BiFeO_3$. From these observations the charge neutrality, the compensation of oxygen octahedron [15] hindering the growth of secondary phases and the signature of magnetoelectric effect are observed when the concentration of Sr exceeds 30% in Sr-doped $BiFeO_3$ [16]. Hence polycrystalline $Bi_{0.6}Sr_{0.4}FeO_{3-\delta}$ is studied here with an intention of getting explicit magnetoelectric property and/or magnetocapacitance effect. Also it is known that magnetization can be enhanced by the presence of oxygen vacancies when metal doping is done [14–17]. This is also a reason for choosing $Bi_{0.6}Sr_{0.4}FeO_{3-\delta}$ for the study, as there will be two contributions to magnetism.

2 Experimental details

Polycrystalline ceramics of $BiFeO_3$ and $Bi_{0.6}Sr_{0.4}FeO_{3-\delta}$ were prepared by the conventional solid-state reaction method. The starting materials Bi_2O_3, Fe_2O_3 and $SrCO_3$ (99.99%) were taken in the stoichiometric proportion and ground intensely for 45 min. These raw materials were then taken in an alumina crucible and calcined at 600 °C for 2 h. These mixed powders were then pelletized under a hydraulic pressure of 30 MPa before sintering at 835 °C for 2 h. X-ray diffraction measurements were carried out for the powder sample using the PANalytical X'Pert Pro diffractometer employing *CuKα* radiation ($\lambda = 1.5415$ Å) in a wide scanning range of 10°–90° with a step size of 0.0170 and scanning time at 9.5° per second. Rietveld refinement and the estimation of structural parameters were done using GSAS II software [18]. Dielectric measurements were done with dielectric broadband spectrometer in the frequency range of 10 Hz–1 MHz at ambient temperature (Concept 80 System, Novocontrol GmbH, Germany). Temperature-dependent dielectric measurements were carried from ambient temperature to 450 °C at 10, 50 and 100 kHz with a heating rate of 10 °C/min. The surface morphology and elemental analysis of the sample were investigated using JEOL JSM-6390 scanning electron microscope (SEM) close fitting with an energy dispersive spectroscopy (EDS) at a voltage of 20 KV and with resolution of 1 µm. The magnetization measurements were carried out at room temperature using a Lake Shore VSM7410 vibrating sample magnetometer with a field accuracy of ±0.1 kOe. Low-temperature magnetization measurement (2 K) was carried out using a commercial SQUID magnetometer (Quantum Design, Inc.). The magnetocapacitive effect was analysed from Polytronic Electromagnet HEM 100 along with Lake Shore 425 Gaussmeter up to a field of 5 kOe coupled to ferroelectric loop tracer (Marine India Pvt. Ltd.). The thermo-magnetic analyses were carried out by differential scanning calorimetry (DSC) (NETZSCH DSC 204). The measurements were done in the nitrogen atmosphere at the heating rate of 10 °C/min with an accuracy of ±0.1 °C.

3 Results and discussion

3.1 Structural analysis

X-ray diffraction patterns of $BiFeO_3$ and $Bi_{0.6}Sr_{0.4}FeO_{3-\delta}$ are shown in Fig. 1a. The observed Bragg angles 2θ of $BiFeO_3$ are comparable with standard data (JCPDS# 01-086-1518) of the rhombohedral *R3c* phase. There are minute traces of mullite ($Bi_2Fe_4O_9$) (JCPDS# 00-025-0090) around 27°, 32° and selenite ($Bi_{25}FeO_{39}$) (JCPDS# 00-046-0416) around 28°, 46°. Nevertheless, samples sintered under higher temperature for longer period displays secondary phases [5]. Also the observed X-ray pattern of $Bi_{0.6}Sr_{0.4}FeO_{3-\delta}$ is comparable with standard data (JCPDS# 01-086-0107) of *pm3m* phase. The predominant peaks at (104) and (110) planes of $BiFeO_3$ correspond to the intense peak at 31.9° of $Bi_{0.6}Sr_{0.4}FeO_{3-\delta}$ (Fig. 1b). This could be due to the difference in ionic radius of divalent Sr^{2+} ions (1.26 Å) and the trivalent Bi^{3+} ions (1.17 Å) [19]. As a result, lattice distortion occurs in $Bi_{0.6}Sr_{0.4}FeO_{3-\delta}$ and volume of the unit cell reduces. This induces a structural phase transition from rhombohedral (*R3c*) to cubic phase (*pm3m*). The crystalline sizes of $Bi_{1-x}Sr_xFeO_{3-\delta}$ ($x = 0$ and 0.4) are determined by Scherrer formula by considering the most intense diffraction peak in the XRD pattern [20] given by

$$D = 0.89\lambda/\beta \cos\theta, \quad (1)$$

where D is the crystalline size of the most intense peak, λ is the wavelength of incident radiation (1.5415 Å), β is the full-width half-maximum in radians and θ is the angle of diffraction. In this case, both systems have crystalline sizes as 126 and 99 nm for the most intense peak. Though the peak shifts towards higher angle, the two predominant peaks (104, 110) observed in $BiFeO_3$ is merged and broaden in to a single peak in $Bi_{0.6}Sr_{0.4}FeO_{3-\delta}$. Hence the broadening of the peak is attributed to decrease in crystalline size and increase in lattice strain [21]. Rietveld refinement of $BiFeO_3$ gives the lattice parameter values as $a = b = 5.5736(3)$ Å, $c = 13.8436(1)$ Å and $V = 372.438$ Å^3. The bond angle of Fe–O–Fe along $[0\bar{1}0]$ direction and the bond length of Bi–O for pure $BiFeO_3$ are found to be 155.13 (0)° and 2.573 Å, respectively. In addition to the primary phase, two additional phases $Bi_2Fe_4O_9$ (*Pbam*) and $Bi_{25}FeO_{39}$ (*I23*) are also seen. After several cycles of refinement, the final fractional ratios of *R3c, Pbam* and *I23* phases are found to be 84.8,

Author's personal copy

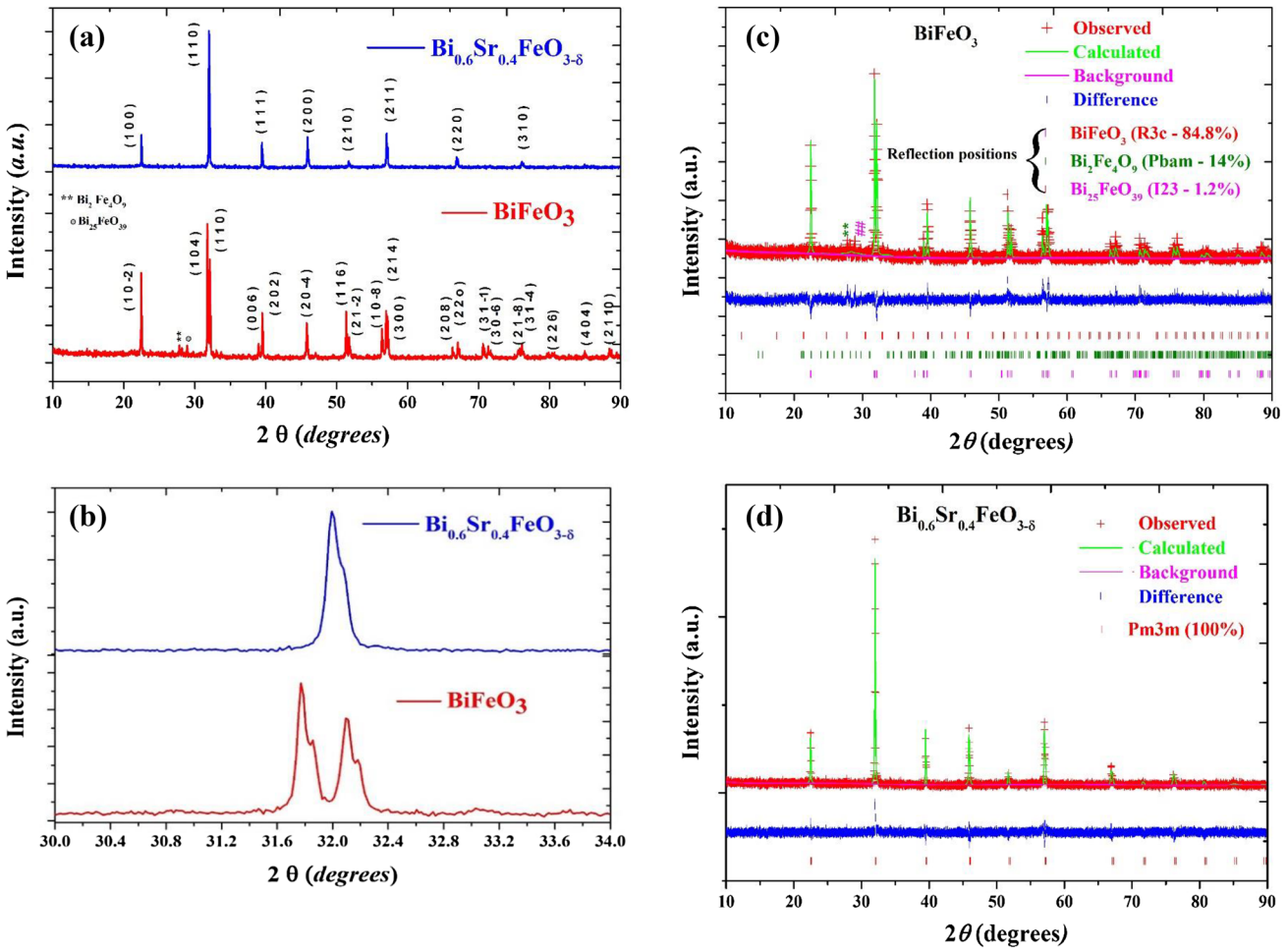

Fig. 1 **a** X-ray diffraction patterns of $BiFeO_3$ and $Bi_{0.6}Sr_{0.4}FeO_{3-\delta}$. **b** Prominent splitting peaks of (104), (110) in $BiFeO_3$ and merged single peak of (110) in $Bi_{0.6}Sr_{0.4}FeO_{3-\delta}$ at 31.9°. Rietveld refinement patterns of **c** $BiFeO_3$ and **d** $Bi_{0.6}Sr_{0.4}FeO_{3-\delta}$. The red plus symbols represent the experimental data whereas calculated pattern is showed as solid green line. The difference pattern between the calculated and experimental data is given as blue solid line. Magenta vertical bars represent the allowed Bragg peak positions for their respective crystal structures while the red and greenish vertical bars indicates secondary phases of the corresponding crystal structure

14 and 1.2%, respectively. The refined lattice parameters of $Bi_{0.6}Sr_{0.4}FeO_{3-\delta}$ are observed to be $a=b=c=3.9436$ Å and $V=61.349$ Å^3. The bond angles of Fe–O–Fe along [0 0 1] direction and the bond length of Bi/Sr–O are found to be 180° and 2.789 Å, respectively. The Rietveld refined parameters of $BiFeO_3$ and $Bi_{0.6}Sr_{0.4}FeO_{3-\delta}$ are listed in Table 1 and their refined patterns are shown in Fig. 1c, d.

3.2 Microstructural analysis

Figure 2a, b shows the microstructural analysis of $BiFeO_3$ and $Bi_{0.6}Sr_{0.4}FeO_{3-\delta}$, respectively. It is found that $BiFeO_3$ crystallizes with an average particulate size of 1.17 µm while $Bi_{0.6}Sr_{0.4}FeO_{3-\delta}$ represents agglomerate particles having unequal axis and the average particle size is found be 0.778 µm [22]. Energy dispersive spectroscopy of $Bi_{0.6}Sr_{0.4}FeO_{3-\delta}$ is shown in Fig. 2c. Table 2 displays the atomic percentages of the elements Bi, Sr, Fe and O as 12.12, 8.33, 23.32 and 56.23, respectively. The oxygen content is calculated based on the atomic percentages obtained from the EDS analysis. The atomic percentages are found to be consistent with stoichiometry 0.52:0.36:1:2.4 of the elements Bi, Sr, Fe and O. A comparison between atomic percentage of Bi^{3+} and Fe^{3+} ions suggests that the Bi^{3+} ions are fewer than Fe^{3+} ions in $Bi_{0.6}Sr_{0.4}FeO_{3-\delta}$ because of the volatilization of Bi^{3+} ions during heat treatment. It is also observed that the oxygen content is found to be 2.4 (instead of 3) which indicates the presence of oxygen vacancies in $Bi_{0.6}Sr_{0.4}FeO_{3-\delta}$. Hence, this is expected to alter the electrical and magnetic properties in $Bi_{0.6}Sr_{0.4}FeO_{3-\delta}$.

Author's personal copy

Table 1 Structural parameters and Rietveld refinement results of $BiFeO_3$ and $Bi_{0.6}Sr_{0.4}FeO_{3-\delta}$

Sample	$BIFeO_3$		$Bi_{0.6}Sr_{0.4}FeO_{3-6}$	
Space group	*R3c*		*Pm3m*	
Lattice parameter	$a=b=5.5736(3)$ Å, $c=13.8436(1)$ Å		$a=b=c=3.9436$ Å	
Interfacial angles	$\alpha=\beta=90°$ $\gamma=120°$		$\alpha=\beta=\gamma=90°$	
	Bi (0, 0, 0)		Bi/Sr (0.5, 0.5, 0.5)	
Atomic positions	Fe (0, 0, 0.2208)		Fe (0, 0, 0)	
	0 (0.4473, 0.0198, 0.9525)		0 (0.5, 0, 0)	
Volume	372.438 Å^3		61.349 Å^3	
Density	8.347 gm/cm^3		7.155 gm/cm^3	
Bond angle	Fe–O–Fe	Bi–O–Bi	Fe–O–Fe	Bi/Sr–O–Bi/Sr
	$[0\bar{1}0]$	[HI]	[000]	$[0\bar{1}0]$
	155.130°	107.73°	180°	90°
Bond length	Fe–O	Bi–O	Fe–O	Bi/Sr–O
	$[0\bar{1}0]$	[HI]	[000]	$[0\bar{1}0]$
	1.9605 Å	2.573 Å	1.9712 Å	2.789 Å
	$\chi^2=1.241$		$\chi^2=1.060$	
	wRp=0. 1743		wR_p=0.1381	
R-factors	$R_p=0.1375$		$R_p=0.1092$	
	$R_F{}^2=0.2332$		$R_F{}^2=0.1432$	

3.3 Magnetic studies

Figure 3a shows *M–H* hysteresis loop of $BiFeO_3$ at ambient temperature. Here the loop varies linearly up to a field of 15 kOe with unsaturated hysteresis confirming antiferromagnetic spin arrangement. The maximum magnetization (at 15 kOe), very small coercive field and remanent magnetization are found to be 0.088 emu/g, 130 Oe and 1.089 memu/g, respectively.

Figure 3b shows the field variation of the magnetization at ambient temperature for $Bi_{0.6}Sr_{0.4}FeO_{3-\delta}$. *M–H* loop resembles a non-linear sigmoid-type variation up to 10 kOe and a further increase in the field shows a linear variation in magnetization approaching a magnetic saturation at 15 kOe due to weak ferromagnetic behaviour. The maximum magnetization for $Bi_{1-x}Sr_xFeO_{3-\delta}$ ($x=0$, 0.4) are found to be 0.088 and 5.097 emu/g, respectively. Figure 5c shows the variation of the bond angle (Fe–O–Fe), bond length (Fe–O) with maximum magnetization (emu/g) for $Bi_{1-x}Sr_xFeO_{3-\delta}$. It is observed that, as the bond angle and bond length increase the maximum magnetization also increased. The average magnetic moment per formula unit in Bohr magneton of $BiFeO_3$ and $Bi_{0.6}Sr_{0.4}FeO_{3-\delta}$ are calculated using the relation

$$\mu_B(f.u.) = \frac{M \times M_s}{5585}, \tag{2}$$

where M is the molecular weight of the sample and M_s is the saturation magnetization [23]. Here the maximum magnetization of $Bi_{0.6}Sr_{0.4}FeO_{3-\delta}$ is nearly saturated because of the coexistence of ferromagnetic and antiferromagnetic behaviours. However, we can use this equation to roughly estimate the magnetic moment of samples. The average magnetic moment per *Fe* ion of $BiFeO_3$ and $Bi_{0.6}Sr_{0.4}FeO_{3-\delta}$ are found to be 0.0049 and 0.241 μB/Fe, respectively. These magnetic moments are compared to the spin only magnetic moment of 4.9 μB/Fe^{2+}($S=2$), 5.916 μB/Fe^{3+} ($S=5/2$) and 0/Fe^{4+} ions ($S=0$) in spiral spin structure. This leads to the conclusion that $Bi_{0.6}Sr_{0.4}FeO_{3-\delta}$ shows weak ferromagnetic behaviour with relatively higher magnetic moment per Fe^{3+} ion and/or Fe^{2+} ion than the host $BiFeO_3$ [24]. The coercive field and remanent magnetization are found to be 3.4 kOe and 2.86 emu/g ($M_r=0.135$ μB/Fe), respectively. The increase in magnetization from the host may be due to two reasons (1) due to the divalent substitution $Bi_{0.6}Sr_{0.4}FeO_{3-\delta}$ may possess two different valence states, viz., Fe^{2+}/Fe^{4+} and Fe^{3+} or oxygen ion vacancies. As a result they may suppress the spiral spin ordering and lead to increase in the total magnetization [25] (2) due to the finite size effect of $Bi_{0.6}Sr_{0.4}FeO_{3-\delta}$, the particle size is reduced and the predominant peaks are slightly shifted from the position of host $BiFeO_3$ as revealed from SEM and XRD analysis [26]. The increase in coercive field of $Bi_{0.6}Sr_{0.4}FeO_{3-\delta}$ may be due to the phase transition from rhombohedral (*R3c*) to cubic (*Pm3m*) phase in $Bi_{0.6}Sr_{0.4}FeO_{3-\delta}$. This causes transformation from inhomogeneous to homogeneous spin structure, thereby decreasing the magnetic anisotropy [26, 27].

Figure 3c shows the field variation of the magnetization at 2 K for $Bi_{0.6}Sr_{0.4}FeO_{3-\delta}$.The saturation magnetization, remanent magnetization and coercive field are found to be 12.378 emu/g (0.586 μB/Fe), 5.36 emu/g (0.254 μB/*Fe*)

Author's personal copy

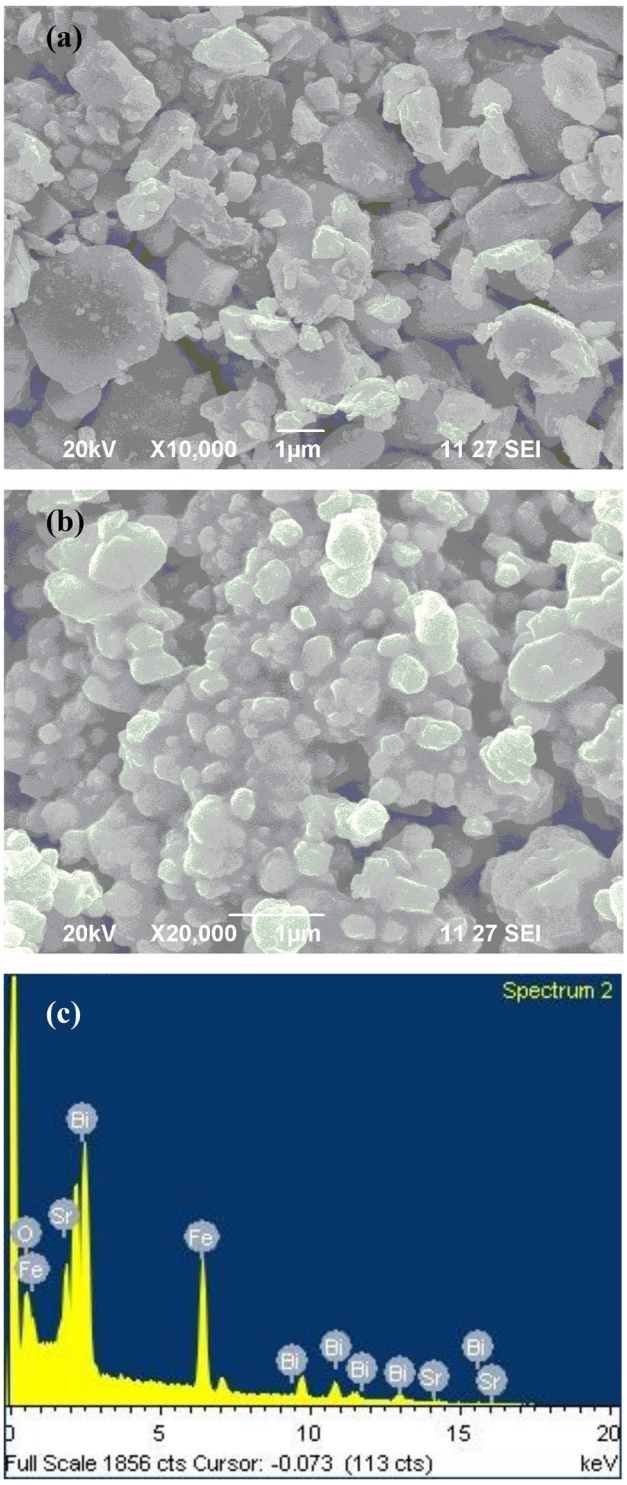

Fig. 2 Microstructural analysis of **a** $BiFeO_3$ and **b** $Bi_{0.6}Sr_{0.4}FeO_{3-\delta}$. **c** Energy dispersive spectra of $Bi_{0.6}Sr_{0.4}FeO_{3-\delta}$

and 1.8 kOe, respectively. Here the coercive field at lower temperature (1.4 kOe) is smaller than at room temperature (3.4 kOe).

Table 2 Atomic percentage analysis of $Bi_{0.6}Sr_{0.4}FeO_{3-\delta}$

	Atomic percentage			
Sample composition	Bismuth	Strontium	Iron	Oxygen
$Bi_{0.6}Sr0.4FeO_{3-\delta}$	12.12	8.33	23.32	56.23

According to Hussain et al. [17], the decrease of coercivity at lower temperatures is the signature of magnetoelectric coupling which results in reduced effective single ion anisotropy and reduced coercivity. Wang et al. [27] explains the magnetoelectric coupling via Dzyaloshinskii–Moriya (DM) interaction using Ginzburg–Landau free energy and found that the effective anisotropy energy of the multiferroic is reduced by the effect of magnetoelectric coupling in *Ba*-doped $BiFeO_3$.

Hence the largest difference between high- and low-temperature magnetizations and coercive fields may be visualized as due to strong magnetoelectric coupling.

3.4 Dielectric studies

Figure 4a displays the frequency-dependent real part of the dielectric permittivity ε_r' of $BiFeO_3$ and $Bi_{0.6}Sr_{0.4}FeO_{3-\delta}$ at ambient temperature where the dielectric permittivity (ε_r') shows a higher value at lower frequencies irrespective of the temperature due to the formation of interfacial space charges near the electrodes. At higher frequencies the plot shows a decreasing trend corresponding to the electrical relaxation of the bulk sample and finally approaching saturation at frequencies above 1 MHz giving the high-frequency dielectric permittivity (ε_∞) of the material [28]. The dielectric permittivities (ε_r') of $BiFeO_3$ and $Bi_{0.6}Sr_{0.4}FeO_{3-\delta}$ at 1 *MHz* are found to be 16 and 74 which are comparable to the reported values of Varshney et al. [13] and Hussain et al. [17]. These space charges arise primarily due to dipoles at the oxygen (V_O^{2-}) and bismuth (V_{Bi}^{3+}) vacancies during doping of cations and follow the applied field at lower frequencies. As a result the dielectric loss is larger at lower frequencies (Fig. 4b). At higher frequencies they are unable to follow the applied field and experience dipole relaxation [29]. Hence factors such as crystallinity, grains, etc., may affect the dielectric permittivity at these frequencies. According to Varshney et al. [13] the large value of ε_r' in $BiFeO_3$ is mainly due to the creation of oxygen vacancies or by conversion of Fe^{3+} to Fe^{2+}/Fe^{4+}. Hence it is expected that the charge imbalance might be compensated either by the interaction of O^{2-} ions through hopping conduction mechanism or by the creation of oxygen vacancies that might help ordering of the oxygen octahedron.

Figure 4d shows the temperature-dependent dielectric permittivity of $Bi_{0.6}Sr_{0.4}FeO_{3-\delta}$ at 10, 50, and 100 kHz, respectively. It is observed that ε_r' starts increasing with

Author's personal copy

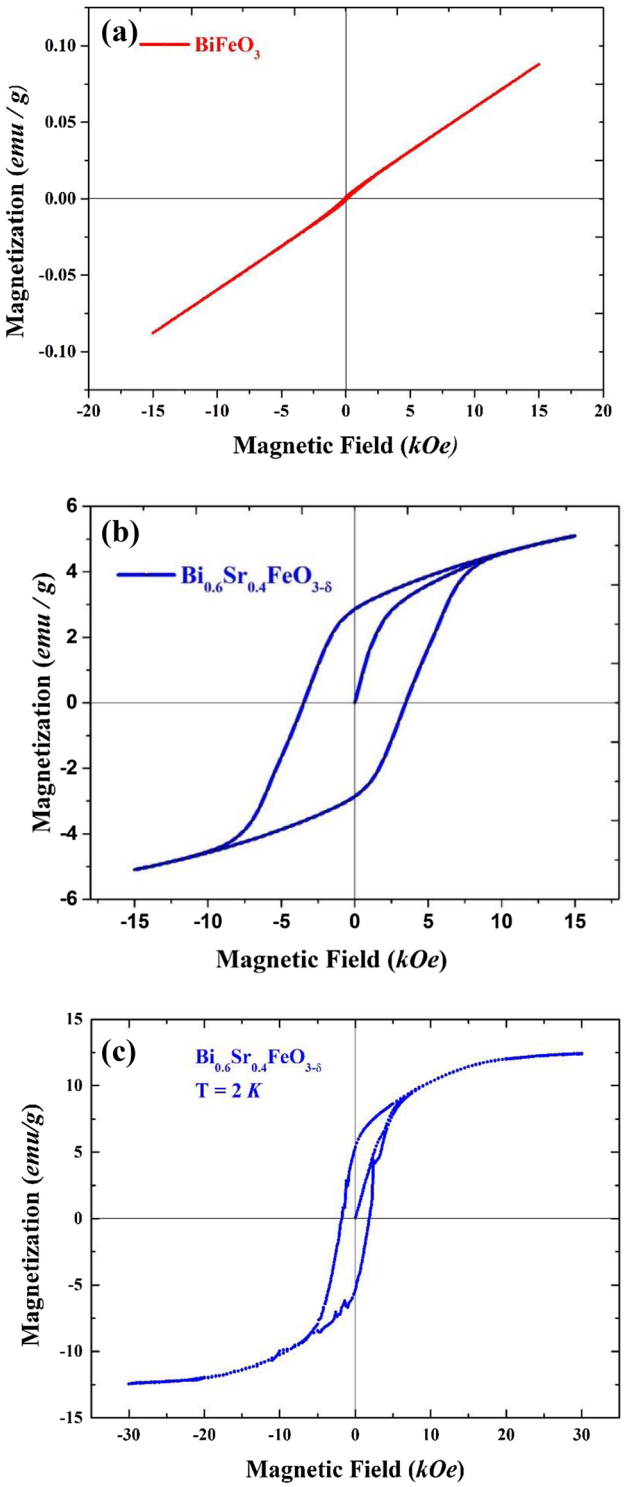

Fig. 3 Ambient temperature magnetization as function of applied magnetic field for **a** $BiFeO_3$ and **b** $Bi_{0.6}Sr_{0.4}FeO_{3-\delta}$. **c** Magnetization as a function of applied magnetic field for $Bi_{0.6}Sr_{0.4}FeO_{3-\delta}$ at $T = 2$ K

the increase in temperature from ambient to 450 °C and an anomaly is observed at 321 °C at all the measured frequency ranges due to weak ferromagnetic transition temperature. This anomaly is a signature of magnetoelectric ordering and the vicinity of the peak slowly diminishes on increasing the frequency due to suppression of magnetic ordering on electric order as predicted by Landau–Devonshire on phase transition [13]. This result is comparable with some of the reported rare earth-doped $BiFeO_3$ polycrystalline ceramics [30]. It is also to be noted that the temperature-dependent dielectric permittivity of $BiFeO_3$ at 10, 50, and 100 kHz shows an increasing trend till the range of temperature measurement as shown in Fig. 4c and needs further investigations.

4 Magnetocapacitive effect

The variation of capacitance with the applied magnetic field is measured from the magnetic field coupled ferroelectric tester at ambient temperature [31]. The magnetocapacitance (MC) effect is calculated from the relation

$$\mathrm{MC}\% = \frac{C_{(H)} - C_{(0)}}{C_{(0)}} \times 100, \tag{3}$$

where $C_{(H)}$ and $C_{(0)}$ are the capacitances in the presence and absence of the applied magnetic field. The magnetocapacitance effect of $BiFeO_3$ and $Bi_{0.6}Sr_{0.4}FeO_{3-\delta}$ are found to be 0.4 and 5.3% at a field of 4 kOe as shown in Fig. 5a. The magnetocapacitive effect is found to be enhanced in $Bi_{0.6}Sr_{0.4}FeO_{3-\delta}$ than in bare $BiFeO_3$. This effect is based on the qualitative explanation put forward by Palkar et al. [32]. According to Palkar et al., when external magnetic field is applied to these materials, the materials are strained. This strain induces a stress on the piezoelectric $BiFeO_3$ which generates the electric field. This field could orient the ferroelectric domains leading to an increase in polarization value and hence the magnetocapacitive effect. According to Kumar et al. [33], magnetocapacitance effect is the signature of magnetoelectric coupling present in the system. Here on Sr doping the coupling effect increases thereby enhancing the magnetocapacitive effect. This shows that this $Bi_{0.6}Sr_{0.4}FeO_{3-\delta}$ material is a potential material for coupling electrical and magnetic ordering and is suitable for application in magnetic storage media [34].

5 Discussion

Even though works are available in the literature to show magnetoelectric behaviour in Sr-doped $Bi_{1-x}Sr_xFeO_3$ [12, 13, 17], all the earlier works are up to the Sr concentration of $x = 0.3$, as there is a phase transition above this concentration. Although, the antiferromagnetic nature of $BiFeO_3$ is an obstacle for its practical applications in the present work, this is overcome by increasing the concentration of oxygen vacancies as $O_{1-\delta}$ and by doping Sr to 40%. Here

Author's personal copy

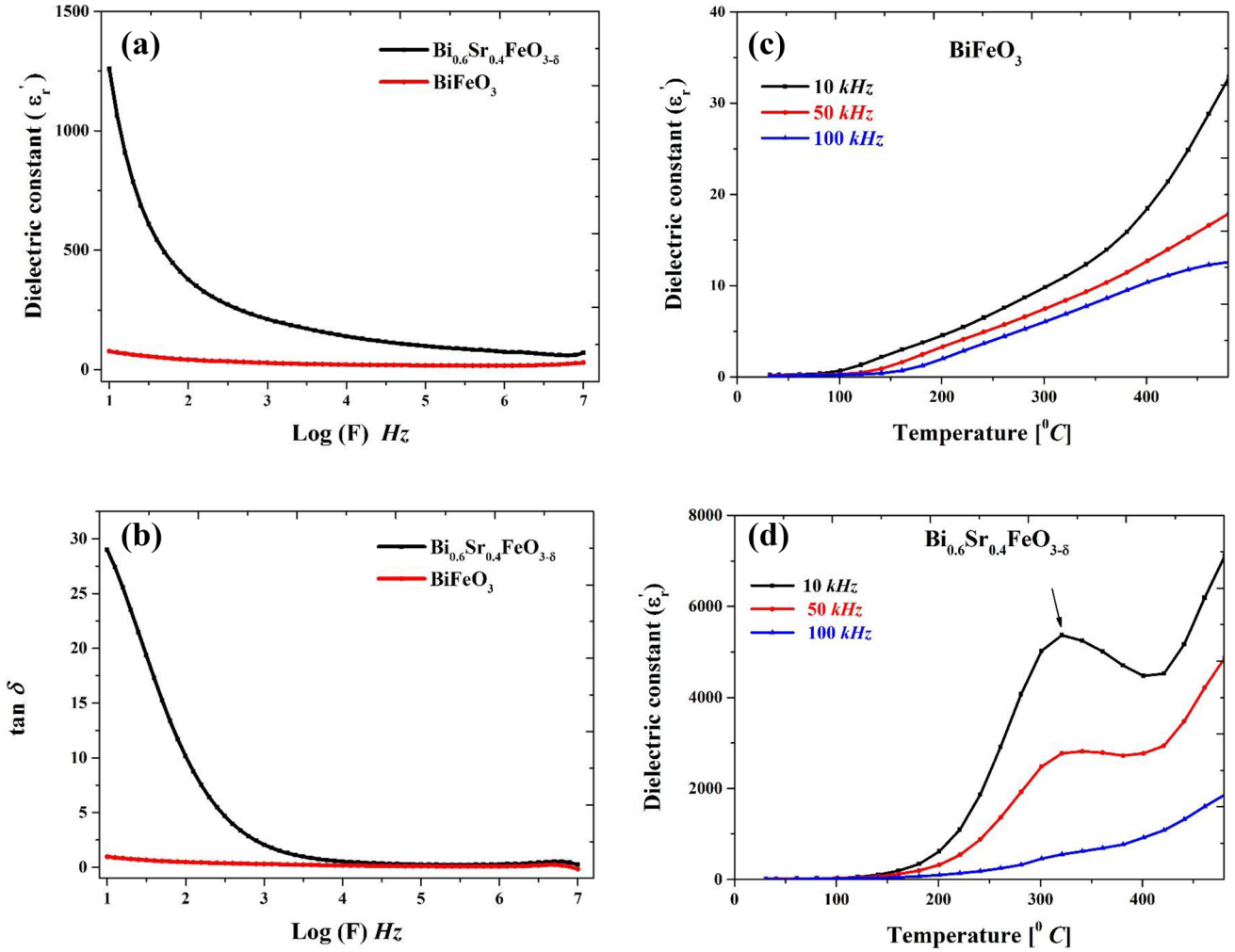

Fig. 4 **a** Frequency-dependent of dielectric permittivities of $BiFeO_3$ and $Bi_{0.6}Sr_{0.4}FeO_{3-\delta}$. **b** Frequency-dependent dielectric losses (tan δ) of $BiFeO_3$ and $Bi_{0.6}Sr_{0.4}FeO_{3-\delta}$. **c** Temperature-dependent dielectric permittivity of $BiFeO_3$. **d** Temperature-dependent dielectric permittivity of $Bi_{0.6}$ $Sr_{0.4}FeO_{3-\delta}$. Arrow indicates the dielectric anomaly at 321 °C

it is found that at about 320 °C, a well stabilized magnetoelectric behaviour is observed in comparison with the earlier works. If this anomaly is particularly due to magnetoelectric coupling, then it may leave its imprint in a differential scanning calorimetry (DSC) measurement. Hence DSC was performed in the region nearer to the observation of Néel temperature (Fig. 5b). An anomaly is observed around 370 °C in $BiFeO_3$ corresponding to the ferromagnetic Néel temperature (T_N), while $Bi_{0.6}Sr_{0.4}FeO_{3-\delta}$ shows the anomaly at 302 °C corresponding to the ferromagnetic transition temperature. Hence it is believed that the anomaly observed in temperature-dependent dielectric permittivity is due to the intrinsic magnetoelectric coupling in $Bi_{0.6}Sr_{0.4}FeO_{3-\delta}$ ceramic. Also a ferromagnetic transition is expected towards room temperature in Sr-doped $BiFeO_3$. Most of the works reported in literature on Sr-doped $BiFeO_3$ are mainly focused on electrical, structural and magnetic properties, but the works on magnetocapacitive effect in Sr-doped $BiFeO_3$ are very sparse. Hence the present work on the magnetocapacitance effect in this composite will be useful for the future works and applications.

Valant et al. [35] investigated the peculiarities of a solid-state synthesis of multiferroic polycrystalline $BiFeO_3$ and found that the oxygen vacancies and formation of impurity phases are difficult to eliminate because of the complex binary mixture between Bi_2O_3 and Fe_2O_3 phases in solid-state route. Hence oxygen vacancy is an intrinsic property of the $BiFeO_3$ system.

In general, the impurity phases ($Bi_2Fe_4O_9$ and $Bi_{25}FeO_{40}$) arising from very low level of doping would affect the microscopic properties of $BiFeO_3$ and not the macroscopic properties. For example, in XRD pattern it is found that a few of the Bragg peaks correspond to the impurity phase ($Bi_2Fe_4O_9$) to the tune of 14%. These peaks have not drastically affected

Author's personal copy

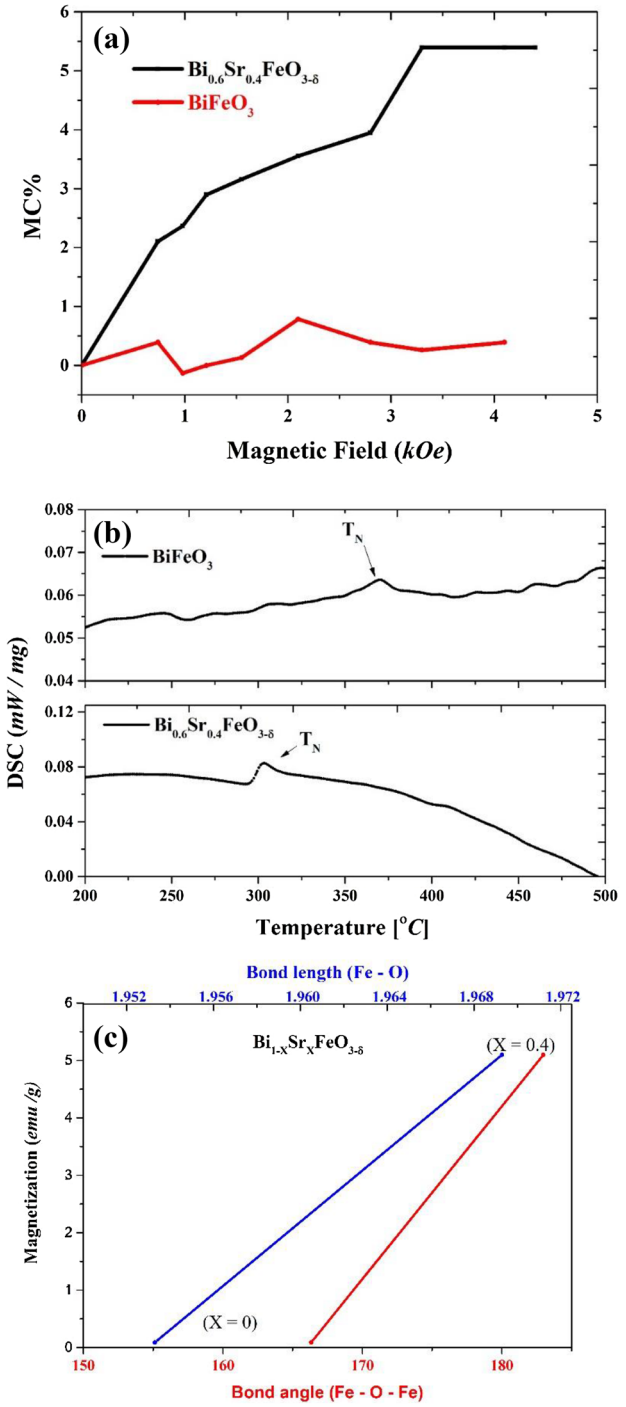

Fig. 5 **a** Ambient temperature magnetocapacitive effect of $BiFeO_3$ and $Bi_{0.6}Sr_{0.4}FeO_{3-\delta}$. **b** DSC curves of $BiFeO_3$ and $Bi_{0.6}Sr_{0.4}FeO_{3-\delta}$. Arrow indicates the Néel temperature of $BiFeO_3$ and $Bi_{0.6}Sr_{0.4}FeO_{3-\delta}$ at 370 and 302 °C, respectively. **c** Variation of the bond angle (Fe–O–Fe), bond length (Fe–O) with maximum magnetization (emu/g) for $Bi_{1-x}Sr_xFeO_{3-\delta}$ ($x = 0, 0.4$) ceramics

the lattice parameters of the host system. So it is expected that there will not be any change in thermal properties. Similarly, ferromagnetic hysteresis loop does not show such variations because the impurity phases such as $Bi_2Fe_4O_9$ and $Bi_{25}FeO_{40}$ are paramagnetic at room temperature. Contrarily, the dielectric constant is low at higher frequencies. This is because these impurity phases ($Bi_2Fe_4O_9$ and $Bi_{25}FeO_{40}$) create charge defects and/or oxygen vacancies thereby degrading the dielectric behaviour. However, introducing Sr in $BiFeO_3$ eliminates such secondary phases and help in tuning the properties of $Bi_{0.6}Sr_{0.4}FeO_{3-\delta}$.

When Sr is doped with $BiFeO_3$ the cycloid spin arranged in *R3c* phase gets suppressed with increase the oxygen vacancies. This changes the Fe coordination ($FeO_{6-\delta}$) and its valence state (Fe^{2+}/Fe^{3+}). In fact the Fe coordination from octahedral to tetrahedral induces a significant structural distortion, thereby collapsing the spatial spin structure [36]. Hence there is a change in bond angle. Similarly, ferroic order in $BiFeO_3$ is due to stereochemical $6s^2$ lone pair of Bi^{3+} ions. Doping with Sr^{2+} will distort the cation spacing between the oxygen octohedra and alter the long-range ferroelectric order. The doping and size contributions to the edge shift due to variation in the number of electrons in valence band and the strain cause the change in bond length. Hence the bond length and bond angle deviate from the host $BiFeO_3$.

6 Conclusion

X-ray diffraction and Rietveld refinement of polycrystalline $BiFeO_3$ and $Bi_{0.6}Sr_{0.4}FeO_{3-\delta}$ showed rhombohedral phase (*R3c*) for $BiFeO_3$ and a *pm3m* phase for $Bi_{0.6}Sr_{0.4}FeO_{3-\delta}$. Microstructural analysis of $Bi_{0.6}Sr_{0.4}FeO_{3-\delta}$ reflects a decrease in particle size due to the influence of Sr in $BiFeO_3$. The maximum magnetizations of $Bi_{0.6}Sr_{0.4}FeO_{3-\delta}$ and $BiFeO_3$ are found to be 5.097 and 0.088 emu/g, respectively. The increase in magnetization may be due to weak ferromagnetic behaviour that may arise due to the suppression of modulated spin structure by Fe^{2+}/Fe^{4+} and Fe^{3+} valence ions and by finite size effect. Temperature-dependent dielectric permittivity of $Bi_{0.6}Sr_{0.4}FeO_{3-\delta}$ shows an anomaly at 321 °C at all higher frequencies due to magnetoelectric coupling in this composite. DSC studies and low-temperature magnetization supports the above result. The magnetocapacitance effect is found to be enhanced in $Bi_{0.6}Sr_{0.4}FeO_{3-\delta}$ than in bare $BiFeO_3$ and hence this composite is suitable for magnetic storage media applications.

Acknowledgements One of the authors (RR) would like to thank the research centres: Sophisticated Analytical Instrument Facility, Indian Institute of Technology Madras, Chennai, for VSM and DSC studies; Department of Physics, Alagappa University, Karaikudi, for the X-ray diffraction measurements; Department of Nanoscience and Technology, Karunya University, Coimbatore, for SEM analysis. Author KR acknowledges UGC, Govt. of India, for emeritus scheme.

Author's personal copy

References

1. W. Eerenstein, N.D. Mathur, J.F. Scott, Nature **442**, 759 (2006)
2. M. Fiebig, J. Phys. D Appl. Phys. **38**, R123 (2005)
3. F. Sosnowska, T.P. Neumaier, E. Steichele, J. Phys. C Solid State Phys. **15**, 4835 (1982)
4. A.K. Pradhan, K. Zhang, D. Hunter, J.B. Dadson, G.B. Loiutts et al., J. Appl. Phys. **97**, 093903 (2005)
5. T.D. Rao, T. Karthik, A. Srinivas, S. Asthana, Solid State Commun. **152**, 2071 (2012)
6. F.P. Ianculescu, P. Gheorghiu, O. Postolache, L. Oprea, Mitoseriu, J. Alloys Compd. **504**, 420 (2010)
7. Reetu, A.Agarwal, S.Sanghi, Ashima, J. Appl. Phys. **110**, 073909 (2011)
8. Y. Zhang, H. Zhang, J. Yin, H. Zhang, J. Chen, W. Wang, G. Wu, J. Magn. Magn. Mater. **322**, 2251 (2010)
9. A.R. Makhdoom, M.J. Akhtar, M.A. Rafiq, M.M. Hassan, Ceram. Int. **38**, 3829 (2012)
10. J. Ray, A. Biswal, S. Acharya, V. Ganesan, D. Pradhan, P. Vishwakarma, J. Magn. Magn. Mater. **324**, 4084 (2012)
11. P. Singh, Y.A. Park, K.D. Sung, N. Hur, J.H. Jung, W.-S. Noh, J.-Y. Kim, J. Yoon, Y. Jo, Solid State Commun. **150**, 431 (2010)
12. S.K. Mandal, T. Rakshit, S.K. Ray, S.K. Mishra, P.S.R. Krishna, A. Chandra, J. Phys. Condens. Matter. **25**, 055303 (2013)
13. D. Varshney, A. Kumar, J. Mol. Struct. **1038**, 242 (2013)
14. B. Kundys, A. Maignan, C. Martin, N. Nguyen, C. Simon, Appl. Phys. Lett. **92**, 112905 (2008)
15. S. Thakur, O. Pandey, K. Singh, Ceram. Int. **40**, 16371 (2014)
16. K. Balamurugan, N.H. Kumar, P.N. Santhosh, J. Appl. Phys. **105**, 07D909 (2009)
17. S. Hussain, S. Hasanain, G.H. Jaffari, N.Z. Ali, M. Siddique, S.I. Shah, J. Alloys Compd. **622**, 8 (2015)
18. B.H. Toby, R.B.V. Dreele, J. Appl. Crystallogr. **46**, 544 (2013)
19. R.D. Shannon, Acta Crystallogr. A **32**, 751 (1976)
20. Reetu, A. Agarwal, S. Sanghi, Ashima, N. Ahlawat, Monica, J. Appl. Phys. **111**, 113917 (2012)
21. G. Arya, R.K. Kotnala, N.S. Negi, J. Am. Ceram. Soc. **97**, 1475 (2014)
22. C.A. Schneider, W.S. Rasband, K.W. Eliceiri, Nat. Methods **9**, 671 (2012)
23. N. Adhlakha, K.L. Yadav, R. Singh, Smart Mater. Struct. **23**, 105024 (2014)
24. V.M. Gaikwad, S.A. Acharya, J. Appl. Phys. **114**, 193901 (2013)
25. S. Hussain, S.K. Hasanain, G.H. Jaffari, S. Faridi, F. Rehman, T.A. Abbas, S.I. Shah, J. Am. Ceram. Soc. **96**, 3141 (2013)
26. S. Layek, H.C. Verma, Adv. Mat. Lett. **3**, 533 (2012)
27. D.H. Wang, W.C. Goh, M. Ning, C.K. Ong, Appl. Phys. Lett. **88**, 212907 (2006)
28. K.W. Wagner, Ann. Phys. **345**, 817 (1913)
29. Z. Dai, Y. Akishig, J. Phys. D Appl. Phys. **43**, 445403 (2010)
30. M. Muneeswaran, R. Dhanalakshmi, N.V. Giridharan, J. Mater. Sci. Mater. Electron. **26**, 6 (2015)
31. S. Chauhan, M. Kumar, S. Chhoker, S.C. Katyal, H. Singh, M. Jewariya, K.L. Yadav, Solid State Commun. **152**, 525 (2012)
32. V.R. Palkar, D.C. Kundaliya, S.K. Malik, S. Bhattacharya, Phys. Rev. B **69**, 212102 (2004)
33. A. Kumar, K.L.Yadav, J. Alloys Compd. **554**, 138 (2013)
34. G.S. Arya, N.S. Negi, Phys. D Appl. Phys. **46**, 095004 (2013)
35. M. Valant, A.K. Axelsson, N. Alford, Chem. Mater. **19**, 5431 (2007)
36. X. Zhang, Y. Sui, X. Wang, J. Tang, W. Su, J. Appl. Phys. **105**, 07D918 (2009)